Rev. Roum. Sci. Techn.– Électrotechn. et Énerg.
Vol. **69**, *2*, pp. 183–188, Bucarest, 2024

PERFORMANCE OF ZINC OXIDE-VANADIUM PENTOXIDE VARISTORS IN MEDIUM VOLTAGE SURGE ARRESTERS

MAGDALENA-VALENTINA LUNGU[1,*], ALINA CARAMITU[1], MIHAI MARIN[1], DELIA PĂTROI[1], VIRGIL MARINESCU[1], CIPRIAN MANEA[1], PETRIŞOR GODEANU[2], ALEXANDRA BARBU[2]

Keywords: Advanced functional materials; Metal oxides; ZnO-V_2O_5 varistors; Medium voltage surge arresters.

Metal oxide varistor (MOV) discs (Ø28 mm × 12 mm) made of 97.5 mol.% zinc oxide (ZnO), and 0.5 mol.% each of vanadium pentoxide (V_2O_5), tin (IV) oxide (SnO_2), antimony(III) oxide (Sb_2O_3), cobalt(II, III) oxide (Co_3O_4), and chromium(III) oxide (Cr_2O_3) additives were produced using powder metallurgy. The obtained MOVs were polycrystalline with high density. This study focused on analyzing the microstructure and mechanical and electrical properties of the MOVs. The developed MOVs had a fine-grained microstructure with an average ZnO grain size of about 10 µm. The Ag-coated MOV discs tested in a range of 100 – 1300 V ac exhibited a leakage current of 0.033 – 1.420 mA and a minimum varistor voltage of 2.37 ± 0.15 kV. After conducting functional tests on Ag-coated MOVs installed in polymer-housed surge arresters, it was found that they are suitable for use in medium voltage arresters with a nominal voltage (U_n) of 25 kV, a continuous operating voltage (U_c) of 12 kV and a leakage current (I_L) of 1 mA.

1. **INTRODUCTION**

Metal oxide varistors (MOVs) are key components in surge arresters, which limit transient overvoltages or surges across power circuits. Metal oxide surge arresters protect electrical equipment and installations in high-, medium-, and low-voltage systems against potentially damaging power surges resulting from faults and lightning strikes [1,2].

MOVs are multicomponent ceramic materials composed of a semiconducting metal oxide (SMO) such as ZnO, SnO_2, or TiO_2, along with MO additives [1–5]. These additives commonly include transition element oxides (TEOs), rare earth oxides (REOs), and other SMOs distinct from the major components utilized in the MOV formulation [2].

MOVs are produced in different formulations, shapes, and sizes using powder metallurgy (PM). MOVs are nonohmic devices with a complex polycrystalline structure and variable electrical resistance (R) to applied voltages [3,6]. MOVs exhibit nonlinear current-voltage (I-V) characteristics, which occur at the grain boundaries (GBs), and display distinct behavior across main regions of the I-V curves [2,6–8]. In the leakage current region, ZnO-based varistors maintain a highly resistive state ($R \leq 10$ GΩ) at low currents ($I < 10$ µA). In contrast, in the upturn region, they exhibit low resistance in the range of 1 – 10 Ω at high currents ($I > 1$ kA). The nonlinear region comprises currents between 10 µA and 1 kA. Above the threshold voltage, also known as the breakdown voltage at 1 mA dc test current (V_{1mA}), the varistor starts to conduct, achieving a high nonlinear coefficient (α) [2,9–11].

The first discoveries on the varistor effect (α of 50) of ZnO-0.5 % Bi_2O_3-1 % Sb_2O_3-0.5 % CoO-0.5 % MnO-0.5 % Cr_2O_3 (mol.%) ceramics sintered at 1350 °C for 1 hour, were conducted by Matsuoka over 53 years ago [3]. Since then, researchers worldwide have continuously developed innovative varistor formulations to enhance their performance in practical applications.

ZnO-based varistors contain a varistor-forming oxide (VFO) such as Bi_2O_3, Pr_2O_3, Pr_6O_{11}, V_2O_5, etc. to induce nonlinearity, along with several varistor-enhancing dopants (VEDs) [2,12–14]. These dopants, selected from TEOs, REOs, and other MOs, are chosen to enhance nonlinearity, conductivity, and stability, as well as to retard or enhance grain growth, among other factors. The type, content, and size of VFO and VEDs, along with GB interface states, greatly influence the electrical properties of MOVs [2,12–14].

Numerous state-of-the-art publications extensively document the fundamental characteristics of ZnO-based varistors, including their electrical properties, physics, chemistry, and microstructure [1,7,8,14].

Disc-shaped ZnO-based varistors, known as ZnO blocks, are among the most widely commercialized MOVs used in surge arrester applications [2,8]. Datasheets detailing ZnO blocks for surge arresters may include characteristics such as dimensions, nominal voltage (U_n), varistor voltage or V_{1mA}, maximum continuous operating voltage (U_c) or rated voltage (U_r), maximum surge current capability (I_{max}), leakage current (I_L), energy absorption capability, response time to a surge event, operating temperature range, etc. However, they usually lack information on the chemical composition of MOVs, which are generically named ZnO blocks. On the contrary, most publications provide details on MOV formulations and some data on processing techniques and specific parameters. However, most investigations mainly focus on the microstructure and electrical properties of MOVs under laboratory conditions.

Commercial ZnO-based varistors primarily contain Bi_2O_3 as a VFO. They exhibit ZnO grain sizes of 10 – 100 µm, a doped GB depletion length ranging from 50 nm to 100 nm, a nonlinear coefficient (α) of 30 – 80, and energy absorption capabilities ≥ 200 J/m^3, among other characteristics [15,16].

The literature provides insufficient data on the development and scalability of MOVs for surge arresters. Moreover, electrical testing under real operating conditions of MOVs installed in surge arresters is generally conducted using commercial ZnO blocks with undefined composition and physical mechanical properties [17–19].

This study presents findings on a novel ZnO-based varistor's microstructure and chemical, mechanical, and electrical properties. The varistor composition includes 97.5 mol.% ZnO as the primary component, 0.5 mol. %

[1] National Institute for Research and Development in Electrical Engineering ICPE-CA (INCDIE ICPE-CA) Bucharest, 313 Splaiul Unirii Street, 030138, Bucharest, Romania
[2] MAIRA MONTAJ SRL, 38A Inovatorilor Street, 012417, Bucharest, Romania
Emails: magdalena.lungu@icpe-ca.ro, alina.caramitu@icpe-ca.ro, mihai.marin@icpe-ca.ro, delia.patroi@icpe-ca.ro
virgil.marinescu@icpe-ca.ro, ciprian.manea@icpe-ca.ro, petre@maira.ro, alexandra.barbu@maira.ro

DOI: 10.59277/RRST-EE.2024.69.2.11

V2O5 as the varistor-forming oxide, and 0.5 mol. % each of SnO_2, Sb_2O_3, Co_3O_4, and Cr_2O_3 as the varistor-enhancing dopants. The electrical tests of MOVs were conducted under laboratory and real operating conditions to evaluate the suitability of the newly developed ZnO-V_2O_5-based varistors for use in medium voltage surge arresters.

2. MATERIALS AND METHODS

High-purity metal oxide powders were utilized as the raw materials for producing MOVs. Table 1 outlines the primary physical properties of the starting powders.

Table 1

Starting metal oxide powders and their primary physical properties

Starting metal oxide powders (producer)	Purity (%)	Particle size (μm)	Molecular weight (g/mol)	Melting point (C)	Density (g/cm^3)
ZnO (Sigma-Aldrich)	99.9	< 5	81.39	1975	5.68
V_2O_5 (Sigma-Aldrich)	≥ 99.6	< 5	181.88	690	3.35
SnO_2 (Merck)	≥ 99	< 5	150.69	1127	6.95
Sb_2O_3 (Carl Roth)	≥ 99	< 5	291.52	656	5.20
Co_3O_4 (Merck)	99.9	< 10	240.80	895	6.11
Cr_2O_3 (Acros Organics)	99.0	< 10	151.99	2435	5.21

The detailed technological process of preparing ZnO-V_2O_5-based composite powders and their consolidation into disc-shaped MOVs with a diameter of 28 mm and a height of 12 mm through powder metallurgy (PM) techniques has been described elsewhere [20]. It is important to mention that green compacts of MOVs were sintered in air at 1200 °C for 2 hours, followed by annealing at 900 °C for 4 hours.

The microstructure and elemental content of MOVs were analyzed with an Auriga Zeiss focused ion beam (FIB) – field emission scanning electron microscope (FESEM) equipped with an Energy Dispersive Spectroscopy (EDS) X-MaxN Silicon Drift Detector at a 5 kV accelerating voltage.

The indentation hardness (H_{IT}), Vickers hardness HV, and elastic modulus (E_{IT}) of the MOVs were determined using a Micro-Combi Tester (MCT^2, CSM Instruments) with a nanoindentation module (NHT^2) and a diamond Berkovich indenter. The tests were conducted following ISO 14577-1 standard [21] and the Oliver & Pharr method [22], with a maximum force (F_{max}) of 300 ± 3 mN in nonlinear loading, an approach speed of the indenter to a disc-shaped MOV of 4000 nm/min, a loading/unloading rate of 600 mN/min, and a holding time of the indenter under F_{max} of 10 seconds. Ten measurements were performed per MOV, and the mean and standard deviation values of H_{IT}, HV, and E_{IT} were reported.

MOVs coated with Ag paste on both circular surfaces were tested in laboratory and real operating conditions. All the electrical tests complied with the standard IEC 60099-4 [23] and the Romanian normative PE 116/94 [24]. A Fluke 435-II three-phase energy and power quality analyzer was used during the measurements.

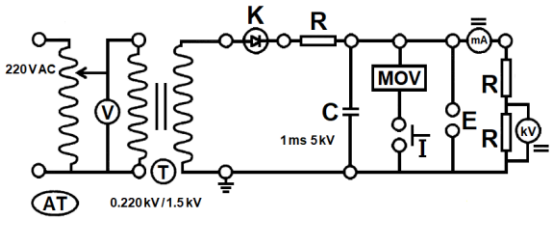

Fig. 1 –Diagram for measuring the electrical resistance of a MOV in DC.

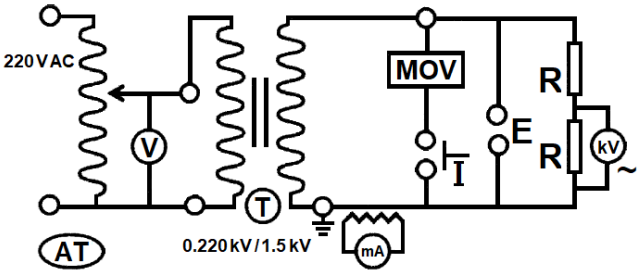

Fig. 2 – Diagram for measuring the leakage current across a MOV in AC.

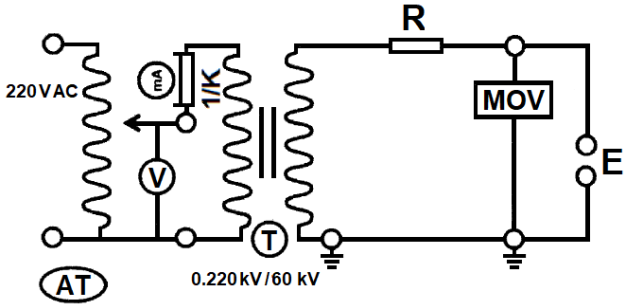

Fig. 3 – Electrical diagram for measuring the minimum varistor voltage of a MOV in ac at the industrial frequency of 50 Hz.

The laboratory electrical testing involved measuring the resistance of MOVs under dc at voltages of 500 V dc and 1000 V dc (Fig. 1), measuring the leakage (conduction) current (I_L) across a MOV in ac at applied voltages of 100 – 1300 V ac (Fig. 2), and determining the minimum varistor voltage (start-to-conduct voltage) in ac, at the industrial frequency of 50 Hz (Fig. 3).

The testing under real operating conditions involved evaluating the performance of MOVs within three polymer-housed gapless surge arresters. The MOV discs were arranged in stacks of 16 pieces per arrester. The electrical tests included measuring the resistive current (I_R) passing across an arrester (Fig. 4), and determining the nominal voltage (maximum breakdown voltage) in dc (Fig. 5) and ac (Fig. 6). The electrical components are symbolized as follows: AT – autotransformer, V – voltmeter, T (HVT) – high voltage transformer, R – resistor, C – capacitor, I – interrupter, kV – kilovoltmeter, mA – miliammeter, MOV – ZnO-V_2O_5-based varistor, FC – filter capacitor, MOSA – metal oxide surge arrester containing MOVs, R_s – shunt resistance, VD – voltage divider, and DSO – digital storage oscilloscope. K is the demultiplication factor (K = 1.5 kV/0.22 kV for the HVT shown in Fig. 1 and 2), and 1/K is the multiplication factor (1/K = 0.22 kV/60 kV for the HVT shown in Fig. 3).

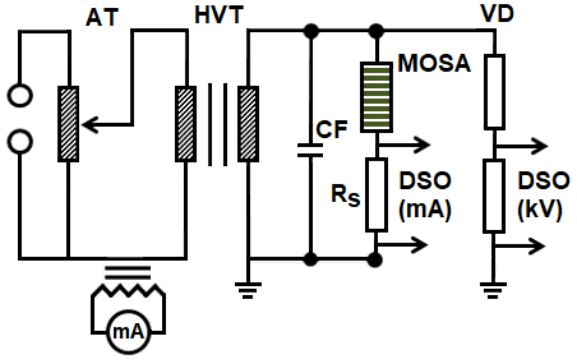

Fig. 4 – Electrical diagram for measuring the resistive current passing across a gapless MO surge arrester (MOSA).

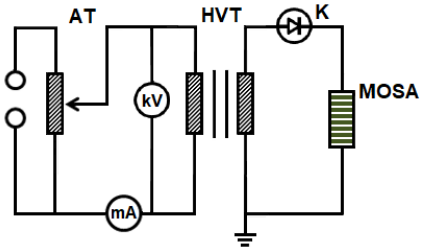

Fig. 5 – Electrical diagram for measuring the breakdown voltage in dc.

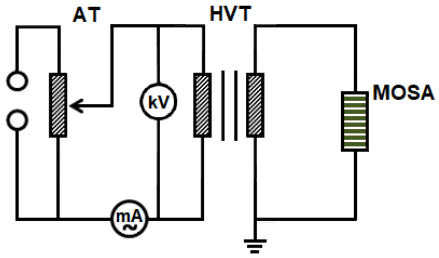

Fig. 6 – Electrical diagram for measuring the breakdown voltage in AC.

3. **RESULTS AND DISCUSSION**

Figure 7 illustrates the macrograph image of the disc-shaped ZnO-V_2O_5-based varistors prepared using PM techniques. It confirms the production of solid blocks of ZnO-V_2O_5-based varistors with a uniform green color, indicating homogeneity in the ceramic materials. Moreover, surface defects like cracks and pits are invisible to the naked eye.

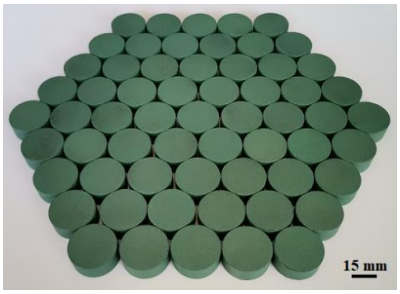

Fig. 7 – Macrograph image of the developed ZnO-V_2O_5-based varistors.

The multicomponent MOVs were polycrystalline and well-densified, with a bulk density of about 5.15 g/cm^3 and low apparent porosity. They also exhibited good dielectric and optical properties, as detailed elsewhere [25].

3.1. MICROSTRUCTURE AND COMPOSITION

Figures 8–10 display the SEM images, EDS spectrum, and EDS layered image of the developed MOVs.

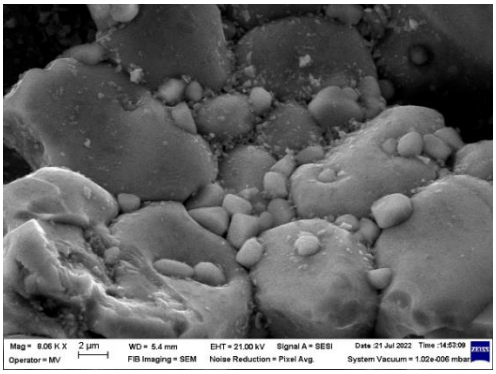

Fig. 8 – SEM secondary electron secondary ion (SESI) image showing a fracture surface of MOVs (8000 ×).

The microstructure of ZnO-V_2O_5-based varistors (Fig. 8 – Fig. 10) consists of microcrystalline grains of ZnO, with an average size of about 10 μm, along with small-sized grains (< 2 μm) resulting from the sintering reactions at high temperature (1200 °C) between ZnO and MO additives. The ZnO grain size of the developed ZnO-V_2O_5-based varistors is consistent with the size range (10 – 15 μm) reported for most commercial ZnO-Bi_2O_3-based varistors [26].

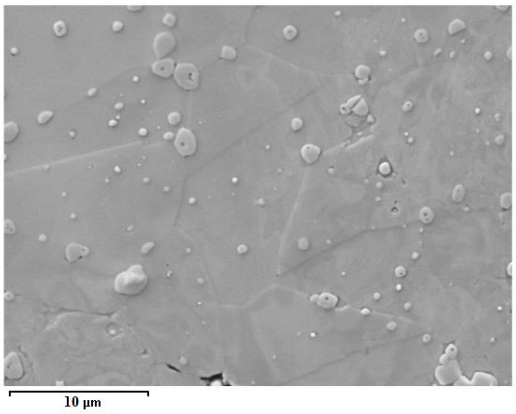

(a)

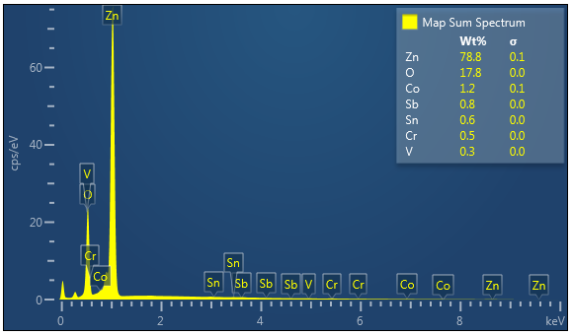

(b)

Fig. 9 – a) SEM secondary electron (SE) image (5000 ×) of an unfractured surface of MOVs; b) corresponding EDS spectrum.

Fig. 10 – EDS layered image (5000 ×) of MOVs.

The SEM micrographs shown in Fig. 8 – Fig. 10 align with the X-ray diffraction results, revealing a predominant ZnO phase with a hexagonal wurtzite structure, characterized by a crystallite size of 138.5 nm, along with a secondary phase containing Zn-Co-Sb-O [25]. Furthermore, in Fig. 8, the intercrystalline fracture surface is observed to coincide with the ZnO grain boundaries (GBs) within the prepared MOVs.

In Fig. 10, it is noticed that V, Sb, and Sn are mostly located at the ZnO GBs, while Co and Cr are associated with both ZnO grains and GBs. The elemental content of the prepared MOVs determined from the EDS analysis (Fig. 9) matched the designed content, although slightly reduced for some metal elements. The decrease in V and Sb can be attributed to the partial volatilization of V_2O_5 and Sb_2O_3 with lower melting points than the sintering temperature of MOVs (1 200 °C) [2]. V_2O_5 is known to exhibit high vapor pressure (≥ 290 Pa) at temperatures over 1 500 K (~1 227 °C), leading to its evaporation during sintering at elevated temperatures [27]. Sb_2O_3 can also vaporize at high temperatures [28]. Moreover, in ZnO-based varistors, it has been found that ZnO, Bi_2O_3 and Sb_2O_3 are the key oxides controlling the sintering reactions at high temperatures, leading to the formation of secondary phases [29,30]. The remaining MO additives used in MOVs can be solidly dissolved in ZnO and incorporated into various secondary phases [30]. The vaporization resistance of ZnO-Bi_2O_3-based systems doped with 0.36 – 0.72 mol·% Bi_2O_3 and 0.72 – 1.44 mol·% Sb_2O_3 increased at high sintering temperatures (1 000 – 1 250 °C) [30]. A similar trend was observed for ZnO-V_2O_5-based systems doped with 0.25 – 0.5 mol·% V_2O_5 and 2 mol·% Sb_2O_3 and sintered at 1 200 °C. The resulting varistors exhibited a main ZnO phase and a $Zn_7Sb_2O_{12}$ spinel secondary phase, which inhibited ZnO grain growth and improved microstructure and electrical properties [12,32].

The density and performance of the newly developed ZnO-V_2O_5-based varistors were enhanced mainly due to V_2O_5, which acted as a sintering aid. During sintering in air at 1 200 °C, forming a V-rich liquid phase facilitated the dispersion of ZnO and other MO particles, promoting GB migration, densification, and enhancing solid-state diffusion processes. Literature studies on ZnO-based varistors doped with 0.5 – 1 mol·% Bi_2O_3 or V_2O_5 also confirmed that liquid-phase sintering induces a ZnO grain boundary structure, leading to nonlinear behavior in varistors [2,33].

In Fig. 10, both the V-rich and the Zn-Co-Sb-O secondary phases are observed to segregate at the ZnO GBs. The segregation of insoluble Sb_2O_3 at the ZnO GB regions occurs due to the larger ionic radius of Sb^{3+} cations (0.076 nm) than that of Zn^{2+} cations (0.074 nm) in the ZnO host lattice. Other metal cations used as dopants in ZnO have ionic radii of 0.069 nm (Sn^{4+}), 0.0615 nm (Cr^{3+}), 0.0545 nm (Co^{3+}), and 0.054 nm (V^{5+}), all smaller than Zn^{2+} cations (0.074 nm) with a coordination number of VI [34]. These metal cations generate more donor states, which improves electron conduction, increases nonlinearity, and reduces the leakage current of ZnO-based varistors [2].

3.2. MECHANICAL CHARACTERISTICS

The newly developed ZnO-V_2O_5-based varistors exhibited an instrumented hardness (H_{IT}) of 2.77 ± 0.20 GPa, a Vickers hardness of 261 ± 16 HV, and an elastic modulus (E_{IT}) of 128 ± 7 GPa. The mechanical properties of these varistors are comparable to those of several commercial ZnO-Bi_2O_3-based varistor blocks (4 kV, class 1) with an average ZnO grain size of 6 – 8 μm [35]. Yoshimura et al. [35] reported hardness values ranging from 1.89 ± 0.09 GPa to 2.26 ± 0.05 GPa, and elastic modulus values between 104.9 ± 1.0 GPa and 115.4 ± 1.8 GPa. The variation in these properties mostly resulted from differences in the type and content of secondary phases and the volume fraction and size of pores in varistors. As expected, MOVs with higher density and a more homogeneous microstructure exhibited better mechanical and electrical properties.

Sedghi et al. [36] disclosed Vickers hardness values of 125 and 251 respectively for ZnO-Bi_2O_3-Sb_2O_3-CoO-Cr_2O_3-MnO-based varistors manufactured with powder metallurgy and micron and nano-sized ZnO powders. However, comparing their material properties is challenging due to numerous factors affecting the properties of ZnO-based varistors [2] and limited data consistency across literature studies.

3.3. ELECTRICAL CHARACTERISTICS

The newly developed varistors demonstrated a significant varistor effect. When subjected to a low voltage of 500 V DC, the varistors exhibited a high resistance of 230 MΩ, indicating a non-conductive state. Increasing the applied voltage to 1000 V dc decreased the resistance to 110 MΩ, indicating a transition to a conductive state. This substantial decrease in resistance suggests the ability of the prepared ZnO-V_2O_5-based varistors to protect against voltage surges.

Table 2 outlines the electrical characteristics of the ZnO-V_2O_5-based varistors measured under ac voltages.

Table 2

Electrical properties of the ZnO-V_2O_5-based varistors under ac voltages

MOV sample no.	Voltage (U_{AC})						$U_{c\ med}$ (kV)
	100 V	200 V	250 V	500 V	1000 V	1300 V	
	Leakage current I_L (mA)						
S1	0.037	0.072	0.088	0.157	0.537	1.200	2.40
S2	0.038	0.075	0.090	0.142	0.583	1.420	2.20
S3	0.033	0.062	0.073	0.111	0.365	1.020	2.50
Mean ± SD	0.036 ± 0.003	0.070 ± 0.007	0.084 ± 0.009	0.137 ± 0.023	0.495 ± 0.115	1.213 ± 0.200	2.37 ± 0.15

At lower ac voltages of 100 V to 250 V, the ZnO-V_2O_5-based varistors exhibited good electrical behavior with low leakage current (I_L) values of 0.033 – 0.090 mA (Table 2), indicating their ability to maintain a high resistance state. Upon increasing the ac voltage to 500 V, the varistors exhibited neutral electrical behavior, with average I_L values of 0.137 ± 0.023 mA. However, at higher ac voltages of 1 000 V and 1 300 V, the varistors displayed poor electrical behavior, suggested by significantly increased I_L values (0.365 – 1.420 mA). Additionally, the average values of the minimum varistor voltage in ac ($U_{c\ med}$) of 2.37 ± 0.15 kV also confirm the good electrical performance of the newly developed varistors, indicating their ability to protect against voltage surges at the industrial frequency of 50 Hz.

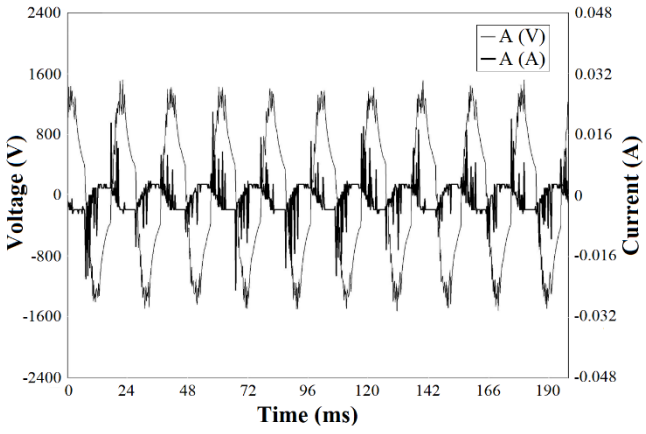

Fig. 11 – Plots of ac voltage and current waveforms over time for a MOV.

Figure 11 presents plots of ac voltage and current waveforms over time, recorded using a Fluke 435-II analyzer in single-phase (A) with neutral mode (AN) at nominal setting (voltage of 1 kV, current of 1 A, frequency of 50 Hz). It shows a voltage dip event, characterized by a rapid deviation from the nominal voltage, captured 187 ms into ac testing of MOVs. However, no transient events were observed during ac testing of MOVs for 1 minute. The maximum root mean square (RMS) current (A_{rms}) was 0.008 A, while the maximum RMS voltage ($V_{rms\ ph\text{-}n}$) was 1.31 kV under AN mode, indicating overvoltage conditions compared to the nominal voltage. The absence of transient events despite overvoltage conditions suggests the efficiency of these MOVs in suppressing voltage spikes during testing.

Figures 12 and 13 depict temperature-time and resistive current-temperature relationships during ac testing of MOVs within gapless surge arresters, maintaining constant voltages (U_c) of 12 kV, 15 kV, and 20 kV, respectively.

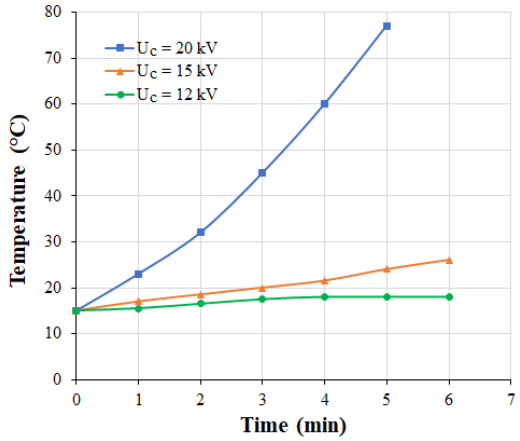

Fig. 12 – Variation of the temperature versus time during ac testing of MOVs in gapless surge arresters at 12 kV, 15 kV, and 20 kV.

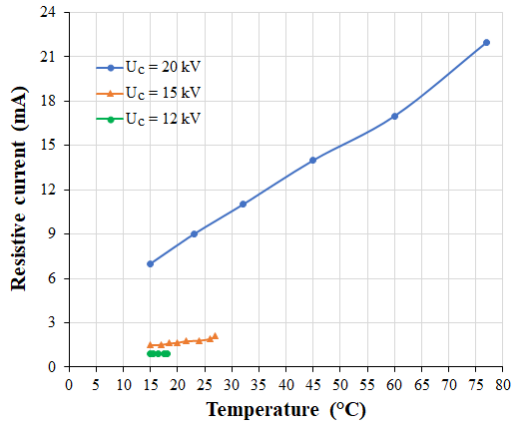

Fig. 13 – Variation of the resistive current versus temperature during ac testing of MOVs in gapless surge arresters at 12 kV, 15 kV, and 20 kV.

As the applied voltage increases from 12 kV to 20 kV, the temperature and resistive current (I_R) of the MOVs exhibited a considerable rise over time. This rise suggests that higher applied voltages increased stress on the MOVs, resulting in higher temperatures and greater resistive currents. The temperature surge was very pronounced under a voltage of 20 kV, with the MOVs reaching a temperature of 77 °C within 5 min. of ac testing, about 5.1 times higher than the initial temperature (15 °C). This temperature rise was mainly due to the increased energy dissipation within the MOVs as they absorb and dissipate excess electrical energy during the surge [1]. The resistive current also increased around 3.1 times, up to 22 mA, with a temperature rise from 15 °C to 77 °C. When subjected to voltages of 12 kV and 15 kV for 6 min., the MOVs attained maximum temperatures of 18 °C and 26 °C respectively. These MOVs exhibited temperature increases of about 3 to 4. times lower than the maximum temperature of 77 °C observed at the higher applied voltage (20 kV). This means lower applied voltages result in less stress on the MOVs and, consequently, lower temperature rises. Additionally, the resistive current decreased considerably within 6 min. testing, with maximum I_R values of 2.1 mA at 27 °C for 15 kV and 0.91 mA at 18 °C for 12 kV. Particularly, under a voltage of 12 kV, the resistive current exhibited minimal variation, ranging between 0.90 mA and 0.91 mA. This steady behavior indicates superior electrical and thermal stability of the MOVs at 12 kV. Therefore, the MOVs are suitable for continuous operation at 12 kV due to their proven reliable performance under this voltage level.

Table 3 presents electrical testing results conducted on MOVs installed in three polymer-housed gapless surge arresters. U_n designates the nominal voltage, U_c represents the continuous operating voltage, K denotes the leakage current (I_L) correction factor (K = 0.8 at 20 °C), and $I_{R\ max}$ indicates the maximum resistive current at 20 °C (Fig. 14).

Table 3

Technical characteristics of the ZnO-V_2O_5-based varistors determined under real operating conditions within gapless MO surge arresters

Sample No.	Tests in DC		Tests in AC			T (°C)	K	U_c (kV) in DC	T_{final} (°C)
	U_n (kV)	I_L (mA)	U_c (kV)	I_L (mA)	$I_{R\ max}$ (mA)				
S1	25.8	NA	20	2.5	20	20	0.8	40	42
S2	26.0	NA	20	2.4	20	20	0.8	41	40
S3	25.5	NA	20	2.5	20	20	0.8	40	41
Mean ± SD	25.8 ± 0.4	NA	20	2.5 ± 0.1	20	20	0.8	40.3 ± 0.7	41 ± 0.7

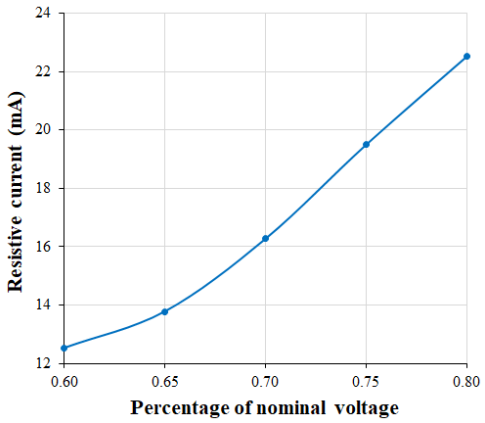

Fig. 14 – Recommended maximum resistive current at 20 °C.

After conducting functional tests on Ag-coated MOVs installed in polymer-housed surge arresters, it was found that they are suitable for use in medium voltage arresters with a nominal voltage (U_n) of 25 kV, a continuous operating voltage (U_c) of 12 kV, and a leakage current (I_L) of 1 mA.

4. CONCLUSIONS

Disc-shaped MOVs made of 97.5 mol·% ZnO, 0.5 mol·% V_2O_5 as the varistor-forming oxide, and 0.5 mol·% each of SnO_2, Sb_2O_3, Co_3O_4, and Cr_2O_3 additives were manufactured through powder metallurgy (PM). The

PM route involved pressing ZnO-V_2O_5-based composite powders into green compacts, sintering at 1200 °C for 2 hours, and annealing at 900 °C for 4 hours. The resulting MOV discs had a final size of 28 mm in diameter and 12 mm in height.

The developed ZnO-V_2O_5-based varistors exhibited a fine-grained microstructure with an average ZnO grain size of about 10 μm, high hardness, and good electrical properties. The Ag-coated ZnO-V_2O_5-based varistors demonstrated the varistor effect under various dc and ac voltages. Testing across a 100 − 1300 V ac voltage range revealed leakage currents between 0.033 mA and 1.420 mA, along with a minimum varistor voltage of 2.37 ± 0.15 kV. These results indicate the ability of these MOVs to protect against voltage surges at the industrial frequency of 50 Hz.

Functional tests conducted on the Ag-coated MOVs installed in polymer-housed surge arresters revealed that the newly developed ZnO-V_2O_5-based varistors are suitable for use in medium voltage surge arresters with a nominal voltage (U_n) of 25 kV, a continuous operating voltage (U_c) of 12 kV, and a leakage current (I_L) of 1 mA.

ACKNOWLEDGMENTS

This work was supported by 327 PED/2020 grant of the Romanian Ministry of Research and Innovation and Digitalization (MCID), CCCDI–UEFISCDI within PNCDI III, 25PFE/2021 grant of the MCID within PNCDI III, Programme 1, and PN 42N/2023 grant of the MCID within NUCLEUS (CORE) Programme.

Received on 20 May 2024

REFERENCES

1. S.C. Pillai, J.M. Kelly, R. Ramesh, D.E. McCormack, *Advances in the synthesis of ZnO nanomaterials for varistor devices*, J. Mater. Chem. C, **1**, *20*, pp. 3268–3281 (2013).
2. M.V. Lungu, *Effects of dopants and processing parameters on the properties of ZnO-V_2O_5-based varistors prepared by powder metallurgy: A review*, Materials, **16**, *10*, 3725 (2023).
3. M. Matsuoka, *Nonohmic properties of zinc oxide ceramics*, Jpn. J. Appl. Phys., **10**, *6*, pp. 736–746 (1971).
4. S.A. Pianaro, P.R. Bueno, E. Longo, J.A. Varela, *A new SnO_2-based varistor system*, J. Mater. Sci. Lett., **14,** *10*, pp. 692–694 (1995).
5. M.V. Lungu, D. Pătroi, V. Marinescu, A. Caramitu, M. Marin, D. Tălpeanu, M. Lucaci, P. Godeanu, *Preparation and study of the optical, electrical and dielectric characteristics of some disc-shaped tin dioxide-based varistors*, Rom. J. Phys., **67**, *7–8*, 610 (2022).
6. J. He, *Metal Oxide Varistors: From Microstructure to Macro-Characteristics*, Wiley-VCH Verlag GmbH & Co. KGaA, Weinheim, Germany, pp. 100–125 (2019).
7. T.K. Gupta, *Application of zinc oxide varistors*, J. Am. Ceram. Soc., **73**, *7*, pp. 1817–1840 (1990).
8. K. Eda, *Zinc oxide varistors*, IEEE Electr. Insul. Mag., **5**, *6*, pp. 28–30 (1989).
9. N. Kularatna, A.S. Ross, J. Fernando, S. James, *Components used in surge protection circuits*, In N. Kularatna, A.S. Ross, J. Fernando, S. James (Edit.), *Design of Transient Protection Systems*, Elsevier, Amsterdam, The Netherlands, 2019, pp. 29–42.
10. L. Hasse, A. Konczakowska, J. Smulko, *Classification of high-voltage varistors into groups of differentiated quality*, Microelectron. Reliab., **49**, *12*, pp. 1483–1490 (2009).
11. K.S. Ganesh, *A review of zinc oxide varistors for surge arrester*, Proceedings of the 2018 4th International Conference on Electrical Energy Systems (ICEES), Chennai, India, pp. 470–474 (2018).
12. H. Hng, K.M. Knowles, *Microstructure and current–voltage characteristics of multicomponent vanadium-doped zinc oxide varistors*, J. Amer. Ceram. Soc., **83**, *10*, pp. 2455–2462 (2000).
13. F. Kharchouche, A. Zebar, *Microstructure and electrical properties of $CaCO_3$-doped ZnO–(Bi_2O_3, Sb_2O_3) based varistor ceramics*, Rev. Roum. Sci. Techn.– Électrotechn. et Énerg. **67**, *4*, pp. 439–444 (2022).
14. L.M. Levinson, H.R. Philipp, E. Sonder, *Interface Effects in Zinc Oxide Varistors*, in J.A. Pask, A.G. Evans (Edit.), *Ceramic Microstructures '86, Materials Science Research*, Springer, Boston, MA, **21**, pp. 665–678 (1987).
15. O. Diwald, *Zinc oxide nanoparticles for varistors*, in O. Diwald, T. Berger (Edit.), Metal Oxide Nanoparticles, Wiley, Hoboken, NJ, USA, pp. 783–807 (2021).
16. A.N.M. Karim, S. Begum, M.S.J. Hashmi, *Role of surface to volume ratio of zinc oxide arrester blocks on the energy absorption capability*, IOP Conf. Ser.: Earth Environ. Sci.**,** **16**, 012008 (2013).
17. C. Rojo Ceballos, F. Chejne, E. Pérez, A. Osorio, A. Correa, *Study of the behavior of low voltage ZnO varistors against very fast transient overvoltages (VFTO)*, Electric Power Syst. Res., **214**, 108937 (2023).
18. F. Munteanu, F.-M. Frigura-Iliasa, E. Cazacu, *About establishing the functional limits of a ZnO varistor based surge-arrester*, Rev. Roum. Sci. Techn.– Électrotechn. et Énerg., **52**, *4*, pp. 443–452 (2007).
19. B. Lončar, M. Vujisić, K. Stanković, P. Osmokrović, *Stability of metal-oxide varistor characteristics in exploitation conditions*, Acta Phys. Pol. A, **116**, *6*, pp. 1081–1084 (2009).
20. M.V. Lungu, C.D. Cîrstea, M. Marin, D. Tălpeanu, A. Caramitu, D. Pătroi, V. Marinescu, G.B. Sbarcea, C.A. Manea, P. Godeanu, A. Barbu, *Process for obtaining some disc-shaped zinc oxide varistors*, RO Patent Application filed with the State Office for Inventions and Trademarks (OSIM), No. A/00741 (2021).
21. ISO 14577-1, *Metallic materials – Instrumented indentation test for hardness and materials parameters – Part 1: Test method* (2015).
22. W.C. Oliver, G.M. Pharr, *An improved technique for determining hardness and elastic modulus using load and displacement sensing indentation experiments*, J. Mater. Res., **7**, *6*, pp. 1564–1583 (1992).
23. IEC 60099-4, *Surge arresters – Part 4: Metal-oxide surge arresters without gaps for a.c. systems*, 2014.
24. PE 116/94, *Normative for tests and measurements performed on electrical installations and equipment*, 1994.
25. M.V. Lungu, A. Caramitu, D. Pătroi, V. Marinescu, G. Sbarcea, M. Lucaci, M. Marin, D. Tălpeanu, P. Godeanu, *Study of disc-shaped ZnO based varistors doped with V_2O_5, Sb_2O_3, Co_3O_4, SnO_2, and Cr_2O_3*, Book of Abstracts of the 10th International Conference of Applied Science (ICAS 2022), Banja Luka, Republic of Srpska, Bosnia & Herzegovina, 25–28 May 2022, p. 65.
26. S. Anas, R.V. Mangalaraja, M. Poothayal, S.K. Shukla, S. Ananthakumar: *Direct synthesis of varistor-grade doped nanocrystalline ZnO and its densification through a step-sintering technique*, Acta Materialia, **55**, *17*, pp. 5792–5801 (2007).
27. T. Shyrokykh, X. Wei, S. Seetharaman, O. Volkova, *Vaporization of vanadium pentoxide from CaO-SiO_2-VO_x slags during alumina dissolution*, Metall. Mater. Trans. B, **52**, *3*, pp. 1472–1483 (2021).
28. T. Karlsson, C. Forsgren, B.-M. Steenari, *Recovery of antimony: A laboratory study on the thermal decomposition and carbothermal reduction of Sb(III), Bi(III), Zn(II) oxides, and antimony compounds from metal oxide varistors*, J. Sustain. Metall., **4**, *2*, pp. 194–204 (2018).
29. M. Peiteado, M.A. de la Rubia, J.F. Fernández, A.C. Caballero, *Thermal evolution of ZnO-Bi_2O_3-Sb_2O_3 system in the region of interest for varistors*, J. Mater Sci., **41**, *8*, pp. 2319–2325 (2006).
30. Y.-W. Lao, S.-T. Kuo, W.-H. Tuan, *Effect of Bi_2O_3 and Sb_2O_3 on the grain size distribution of ZnO*, J. Electroceram., **19**, *2–3*, pp. 187–194 (2007).
31. J. Porcayo-Calderon, J.J. Ramos-Hernandez, C.D. Arrieta-Gonzalez, et al., *Synthesis by hydrothermal treatment of ZnO-based varistors doped with rare earth oxides and their characterization by impedance spectroscopy*, Crystals, **10**, *12*, 1134 (2020).
32. Z. Ming, S. Yu, T.C. Sheng, *Grain growth of ZnO–V_2O_5 based varistor ceramics with different antimony dopants*, J. Eur. Ceram. Soc., **31**, *13*, pp. 2331–2337 (2011).
33. M.L. Arefin, F. Raether, D. Dolejš, A. Klimera, *Phase formation during liquid phase sintering of ZnO ceramics*, Ceram. Int., **35**, *8*, pp. 3313–3320 (2009).
34. R.D. Shannon, *Revised effective ionic radii and systematic studies of interatomic distances in halides and chalcogenides*, Acta Cryst A, **32**, *5*, pp. 751–767 (1976).
35. H.N. Yoshimura, A.L. Molisani, N.E. Narita, J.L.A. Manholetti, J.M. Cavenaghi, *Mechanical properties and microstructure of zinc oxide varistor ceramics*, Mater. Sci. Forum, **530–531**, pp. 408–413 (2006).
36. A. Sedghi, N.R. Noori, *Comparison of electrical properties of zinc oxide varistors manufactured from micro and nano ZnO powder*, J. Ceram. Process. Res., **12**, *6*, pp. 752–755 (2011).